Petroleum Science 23 (2026) 7104–7121

Contents lists available at ScienceDirect

Petroleum Science

journal homepage: www.keaipublishing.com/en/journals/petroleum-science

Original Paper

Fault intelligent identification of seismic data using two-stage method based on coherent attribute

Jiang-Tao Ma [a], Yang Liu [a,*], Suo-Liang Chang [b], Nian-Xu Xi [a], Ding-Ding Deng [a], Xi Di [a]

[a] National Key Laboratory of Petroleum Resources and Engineering, China University of Petroleum (Beijing), Beijing, 102249, China
[b] Taiyuan University of Technology, College of Geological and Surveying Engineering, Taiyuan, 030024, Shanxi, China

ARTICLE INFO

Article history:
Received 15 September 2025
Received in revised form
25 March 2026
Accepted 27 April 2026
Available online 30 April 2026

Edited by Jie Hao

Keywords:
Seismic fault identification
Deep learning
Coherence attribute

ABSTRACT

Faults play a crucial role in the storage and migration of oil and gas, and accurate identification of fault structures is essential for reliable subsurface interpretation and efficient resource development. In recent years, deep learning–based methods have achieved notable progress in fault recognition. However, owing to the pronounced data distribution discrepancy between synthetic and field seismic data, their generalization ability in field scenarios still requires further improvement. Most existing methods adopt single-stage modeling strategies and tend to rely heavily on idealized fault features learned from synthetic data, resulting in limited spatial continuity and reduced stability under complex field geological conditions. To alleviate these limitations, we propose a two-stage fault recognition method guided by coherence-based prior information to enhance model robustness and applicability in synthetic-to-field scenarios. The proposed method simulates the "rough-to-precise" workflow of manual fault interpretation. In the first stage, coherence attributes serve as prior constraints to guide the generation of an initial representation of the overall fault distribution. In the second stage, the fault probability volume from the first stage acts as a fault-related structural prior for fine-scale modeling within localized fault regions. In addition, auxiliary tasks related to fault recognition are introduced at each stage within a multi-task learning framework, enhancing the model's ability to represent fault spatial continuity and structural consistency. Experimental results show that the performance of different baseline methods varies significantly between synthetic and field seismic data. In comparison, the proposed method exhibits improved stability and generalization across multiple field datasets and delineates fault systems with stronger spatial continuity and more reasonable structures. Overall, the proposed method shows practical value under complex geological conditions and provides a reliable solution for field-oriented fault identification.

© 2026 The Authors. Publishing services by Elsevier B.V. on behalf of KeAi Communications Co. Ltd. This is an open access article under the CC BY-NC-ND license (http://creativecommons.org/licenses/by-nc-nd/4.0/).

1. Introduction

Fault identification is a critical step in seismic data interpretation, and its accuracy plays a key role in improving subsequent geological interpretation and hydrocarbon exploration and development. Traditional fault identification methods mainly include coherence-based approaches (Bahorich and Farmer, 1995; Marfurt et al., 1998; Gersztenkorn and Marfurt, 1999), curvature-based methods (Yang et al., 2011; Kazmi et al., 2012), and edge-detection techniques (Al-Dossary and Marfurt, 2003). In addition, some studies have introduced ant colony optimization algorithms into fault identification to suppress noise effects in seismic data, thereby enhancing identification accuracy (Yan et al., 2013; Zhang and Yang, 2015; Li et al., 2019). These methods have demonstrated satisfactory performance in practical applications.

In recent years, with the rapid development of deep learning techniques, deep learning–based fault identification methods have achieved significant improvements in both efficiency and accuracy. Xiong et al. (2018) formulate fault identification as an image classification problem and employ convolutional neural networks (CNNs) to detect faults. Wu et al. (2019a, 2020) propose a synthetic fault data generation strategy and train an end-to-end semantic segmentation–based three-dimensional fault identification model using synthetic datasets, enabling fault detection in 3D seismic volumes. Comparative experiments on field seismic data demonstrate that their approach is more accurate and effective than

* Corresponding author
E-mail address: wliuyang@vip.sina.com (Y. Liu).
Peer review under the responsibility of China University of Petroleum (Beijing).

https://doi.org/10.1016/j.petsci.2026.04.045
1995-8226/© 2026 The Authors. Publishing services by Elsevier B.V. on behalf of KeAi Communications Co. Ltd. This is an open access article under the CC BY-NC-ND license (http://creativecommons.org/licenses/by-nc-nd/4.0/).

traditional methods. Related studies further indicate that CNN-based models achieve both high efficiency and accuracy in fault recognition tasks (Chen and Liu, 2021). Building upon these advances, researchers further introduce attention mechanisms and structural enhancement strategies to improve the representation capability for complex fault structures, including multi-scale feature learning (Jiang and Norlund, 2021; Li et al., 2024), multi-scale attention modules (Gao et al., 2022a, 2022b), knowledge distillation (Wang et al., 2021a), and visual attention mechanisms (Mustafa et al., 2024).

Multi-task learning (MTL) is an inductive transfer learning paradigm that aims to improve model generalization by jointly learning multiple related tasks through shared representations and parallel optimization mechanisms (Rich, 1997). In practical applications, MTL enables the simultaneous handling of multiple correlated tasks, thereby avoiding the need to construct separate models for each task and improving computational efficiency as well as feature reuse. In the context of fault identification, Wu et al. (2019b) simultaneously perform fault detection, structure-oriented smoothing with edge-preserving, and seismic normal estimation within a unified multi-task framework. Furthermore, MTL can enhance the performance of the primary task by introducing auxiliary tasks. For example, Wu et al. (2023) incorporate seismic data reconstruction as an auxiliary task in fault identification, which effectively strengthens the learning capability and performance of the main fault recognition task.

In addition, the Transformer, as a deep learning framework based on the self-attention mechanism, demonstrates a strong capability in global feature modeling (Vaswani et al., 2017). Dosovitskiy et al. (2020) successfully apply the Transformer architecture to the field of natural image analysis, and the Swin Transformer proposed by Liu et al. (2021) achieves remarkable performance in various vision tasks. In the context of fault identification, Tang et al. (2023) introduce Transformer modules into the UNet architecture to realize 2.5D fault recognition by exploiting multi-profile information. Furthermore, Zhou et al. (2024) develop a Swin Transformer–based framework for three-dimensional fault identification, achieving superior recognition performance.

Seismic attributes are important representations reflecting subsurface structural features, which can be used to better understand the underground structures and clearly reveal complex geological characteristics (Bashir et al., 2025). When subsurface structures change, seismic attributes often exhibit noticeable abrupt features, such as anomalous variations in coherence, average energy, phase, and the appearance of high-frequency responses, all of which provide significant indications for fault identification (Bashir et al., 2024, 2025). In recent years, studies have directly used seismic attributes as inputs to deep learning models to achieve automatic fault identification (Huang et al., 2017), demonstrating the effectiveness of seismic attributes in fault characterization. Related research further has incorporated seismic attributes into deep learning architectures, jointly modeling them with seismic data to effectively enhance the model's fault identification performance (Zhang et al., 2024). These studies indicate that seismic attributes not only characterize fault features but can also be regarded as prior information with explicit physical meaning, guiding and constraining the learning process to enhance the model's ability to represent fault structures.

In field seismic data, subsurface structures are highly complex, fault development patterns are diverse, and their spatial distributions often exhibit intricate characteristics such as cross-cutting superposition and multi-scale variability, which poses significant challenges for accurate automatic fault identification. Although deep learning–based methods have made substantial progress in fault identification in recent years, most existing approaches still adopt a single-stage end-to-end modeling strategy. During training, these models tend to learn relatively idealized fault feature representations under synthetic data distributions, and when trained on synthetic data and directly applied to field seismic data, their identification results often exhibit instability and insufficient continuity under complex noise interference and complicated fault geometries, leaving considerable room for further improvement in overall performance. To address these issues, we propose a two-stage fault identification method guided by coherence-attribute priors, which aims to simulate the “rough-to-precise” workflow of manual fault interpretation. The proposed method reconstructs fault identification from a single end-to-end modeling process into two learning stages that collaborate under prior constraints. By introducing different forms of fault-related prior information, the model can achieve more stable and reliable fault identification under complex geological conditions. Compared with existing methods, the main contributions of our work are as follows: 1) A two-stage fault identification framework incorporating coherence-attribute priors is proposed. In the first stage, coherence attributes serve as spatial structural priors to guide the model in initial fault localization, providing stable structural priors for subsequent identification. In the second stage, the fault probability volume obtained from the first stage is used as a fault-related prior and jointly input with the original seismic data into the network, where fault identification is refined under prior guidance, yielding fault results with improved spatial continuity and structural rationality and effectively alleviating the instability of single-stage methods in complex scenarios. 2) In the second stage, the fault probability volume generated in the first stage is introduced as key guiding information, enabling a transition from attribute-based prior constraints to fault-related prior constraints and enhancing the model's perception of fault spatial structures and geometric characteristics. 3) In each stage, auxiliary tasks related to fault identification are incorporated, and a multi-task learning mechanism is employed to strengthen the feature representation of the main task, thereby further improving the spatial continuity and structural integrity of the fault identification results.

2. Method

2.1. Two-stage fault identification method workflow

Currently, most deep learning–based fault identification methods adopt a single-stage end-to-end modeling strategy, in which models are mainly trained on synthetic seismic data and subsequently applied directly to field seismic data. Due to the more complex fault geometries, stronger noise interference in field seismic data, and the pronounced distribution differences between synthetic and field data, the identification results may remain limited in terms of spatial continuity and structural stability. In manual fault interpretation, interpreters usually follow a “rough-to-precise” strategy: major faults are first roughly localized based on global structural characteristics, and local fault details are then refined to enrich structural information and improve identification accuracy. Inspired by this hierarchical interpretation workflow, we propose a prior-guided two-stage fault identification framework, which reconstructs the original fault detection task into two sequential and mutually complementary stages, thereby enhancing model stability and generalization under complex geological conditions.

The overall workflow of the proposed two-stage fault identification method is illustrated in Fig. 1. The method divides fault identification into two stages: rough fault localization and precise

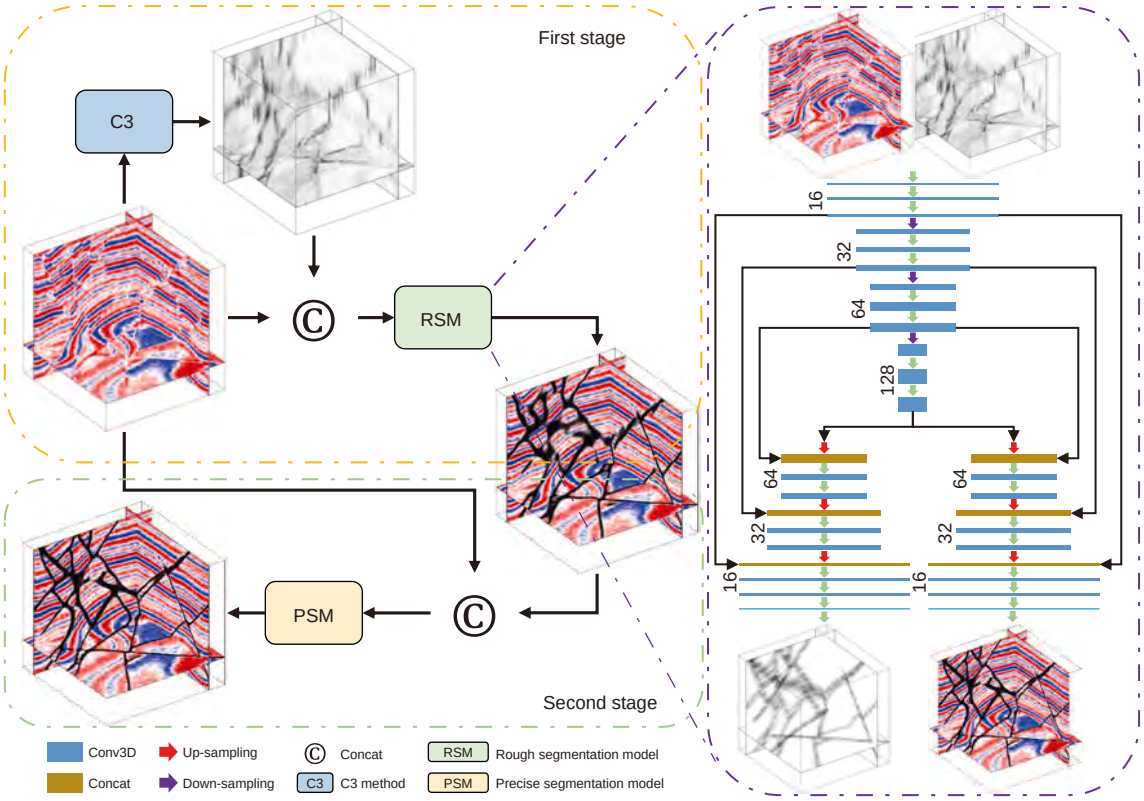


Fig. 1. The workflow of our method framework.

fault delineation. In the first stage, a coherence-guided rough segmentation model (RSM) is constructed. Specifically, coherence attributes are first computed from the original seismic data and are then used together with the seismic data as model inputs. As a fault-related structural prior, coherence attributes explicitly characterize discontinuities within seismic volumes, thereby guiding the model to focus more on potential fault regions. The RSM outputs an initial fault probability volume, which represents the overall spatial distribution trend of faults. In the second stage, the fault probability volume obtained from the first stage is regarded as a fault-enhanced attribute and is jointly input with the original seismic data into a precise segmentation model (PSM). Here, the fault-enhanced attribute serves as a fault-related structural prior, providing spatial guidance on potential fault distributions for the second-stage model. Under the guidance of this prior, the PSM re-models fault structures, allowing the model to focus more on fault-related regions and achieve fine delineation of fault spatial continuity and local structural details. Through the progressive constraints and collaborative processing of the two stages, the model gradually shifts its focus from global fault distribution to local structural details, effectively alleviating the instability and discontinuity issues of single-stage methods in complex scenarios and ultimately producing more refined and stable fault identification results. The detailed architecture of the proposed method is summarized in Table 1.

In principle, both RSM and PSM can employ any model architecture suitable for semantic segmentation tasks. In our work, the models are constructed based on the U-Net architecture. U-Net (Ronneberger et al., 2015) is an encoder–decoder structure model, in which the encoder consists of multiple downsampling modules and the decoder is composed of multiple upsampling modules, with multi-scale feature fusion achieved through skip connections. Owing to its strong feature extraction capability and good adaptability to small-sample datasets, U-Net has been widely applied in the geophysical domain, including tasks such as velocity spectrum picking (Wang et al., 2021b), first arrival picking (Hu et al., 2019), and fault identification (Wu et al., 2019a, 2020). The implementation details of the proposed two-step method are described in the following section.

Table 1
The workflow of our method.

Input: Seismic volume S; Coherence volume C; Ground-truth Y (training only)
Initialize:The network (RSM) parameters θ_1
$P_1 \leftarrow RSM_{\theta_1}(S, C)$
$\mathcal{L}_1 \leftarrow \mathcal{L}(P_1, Y)$
Optimize θ_1 by minimizing $\mathcal{L}_1$
Initialize: The network (PSM) parameters $\theta_2 \leftarrow \theta_1$
$P_2 \leftarrow PSM_{\theta_2}(S, P_1)$
$\mathcal{L}_2 \leftarrow \mathcal{L}(P_2, Y)$
Optimize θ_2 by minimizing $\mathcal{L}_2$
Output: Fault probability volume P_2

2.2. Rough segmentation model

Most of the current deep learning–based fault identification methods typically use only raw seismic data as input. Under complex geological conditions and strong noise interference, such models often struggle to adequately characterize the spatial distribution of faults and their detailed geometric features. Coherence attributes can effectively highlight discontinuities in seismic data and exhibit strong sensitivity to fault structures. As shown in Fig. 2(b), coherence attributes clearly reveal the spatial distribution of major faults, providing reliable structural prior information for fault identification. Therefore, in the rough fault identification stage, coherence attributes are introduced as fault-related

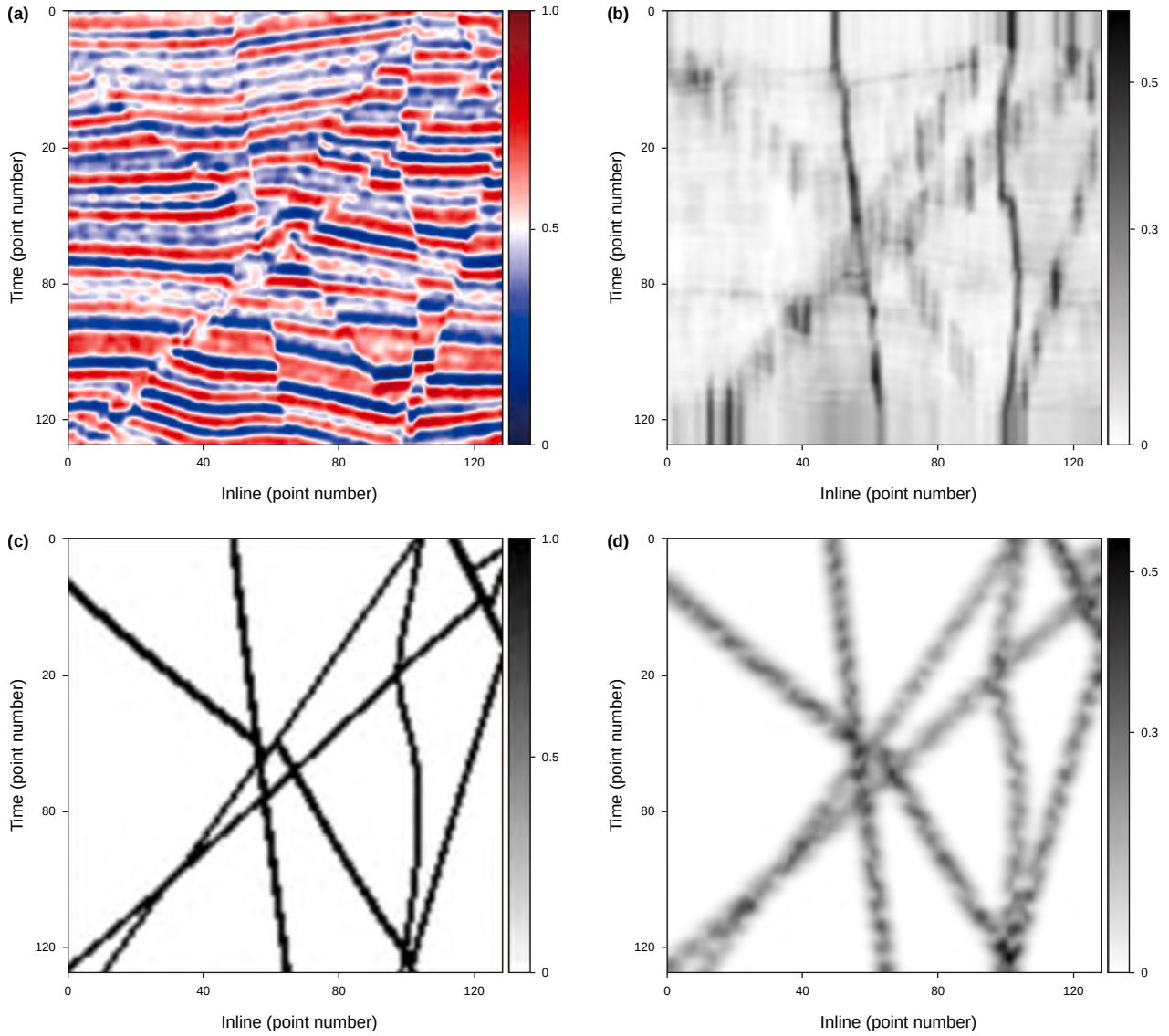


Fig. 2. Schematic diagrams of coherent attributes of seismic data and two types of labels: **(a)** seismic data, **(b)** coherent attribute, **(c)** fault labels, **(d)** auxiliary task labels.

structural priors to enhance the model's perception of the overall fault structure.

For coherence attribute computation, we adopt the eigenstructure-based C3 coherence method (Gersztenkorn and Marfurt, 1999). This method first constructs a local data matrix using a sliding window, then computes its covariance matrix and derives the corresponding eigenvalues, and finally obtains the coherence attribute based on the eigenstructure coherence formulation. To further improve the representation capability and generalization performance of the model, a multi-task learning mechanism is incorporated into the RSM to impose additional constraints on the feature learning process, enabling the model to focus more on features closely related to fault structures. Multi-task learning improves model generalization by sharing feature representations among related tasks (Rich, 1997). However, its effectiveness depends strongly on the correlation among tasks, and information sharing between unrelated tasks may negatively affect model performance (Sebastian, 2017). Therefore, the auxiliary task should be designed to be highly relevant to the main fault identification task, in terms of both physical interpretation and spatial distribution.

The most prominent physical feature of faults is stratigraphic displacement, which is primarily concentrated in regions adjacent to faults, while areas far from faults exhibit weak structural relevance. Based on this observation, we design an auxiliary task that focuses on fault neighborhoods, in which only local data near faults are used as constraints. This strategy strengthens the correlation between the auxiliary and main tasks, fully exploits the synergistic benefits of multi-task learning, and effectively improves both identification accuracy and generalization ability. In contrast to Wu et al. (2023), who adopt global data reconstruction as an auxiliary task, we construct the auxiliary task using local fault-neighborhood data derived from fault physical characteristics, thereby maintaining strong task relevance and further enhancing the model's discrimination capability for fault structures.

The construction procedure of the auxiliary task labels is as follows. First, initial labels are generated from the binary fault labels in synthetic seismic data and then smoothed using a Gaussian filter to obtain a continuous spatial weight distribution. Subsequently, the smoothed weights are multiplied element-wise with the original seismic data to produce regression labels for the auxiliary task. The mathematical formulation is as follows:

$$y_i^{\text{aux}} = G(y_i)\cdot S_i, \tag{1}$$

where, y_i denotes the binary fault labels, S_i represents the seismic data, and $G(\cdot)$ denotes the Gaussian smoothing function. In this study, Gaussian smoothing is applied as a fixed operator, with a consistent smoothing scale across all data. As shown in Fig. 2(d), the constructed auxiliary task labels exhibit high spatial consistency with the fault distribution, highlighting the spatial locations of fault neighborhoods and providing localized structural constraint information.

Based on the above, we construct a coherence-guided Rough Segmentation Model (RSM), whose overall framework is illustrated in the right part of Fig. 1. The inputs of the RSM consist of the original seismic data and the coherence attribute, enabling the model to jointly exploit amplitude information and structural discontinuity information during learning. The RSM adopts a multi-task learning framework, and its outputs include a fault probability volume and the regression results of the auxiliary task. The fault probability volume is used to characterize the overall spatial distribution of faults and provides a stable structural prior for the subsequent precise segmentation stage.

Regarding loss function design, the main fault identification task is formulated as a classification problem, whereas the auxiliary task corresponds to a regression problem. Therefore, different loss functions are adopted for the two tasks and optimized jointly. For the main fault identification task, the sample imbalance issue is significant: as illustrated in Fig. 2(c), black pixels represent fault points and white pixels denote non-fault points, with the latter far outnumbering the former. To alleviate this data imbalance problem, Wu et al. (2019a) employ a balanced cross-entropy loss, which is formulated as follows:

$$\mathcal{L}_{\text{bce}} = -\beta\sum_{i=0}^{N} y_i \log(p_i) - (1-\beta)\sum_{i=0}^{N}(1-y_i)\log(1-p_i), \tag{2}$$

where, $\beta = \sum_{i=0}^{N}(1-y_i)/N$ represents the ratio of non-fault pixels to the total number of pixels, $(1-\beta)$ denotes the fault pixel ratio, y_i indicates the fault label, and p_i refers to the model's output. Wu et al. (2023) use an improved Dice loss function for this task, which is defined as follows:

$$\mathcal{L}_{\text{dice}} = 1 - \frac{2\sum_{i=0}^{N} y_i p_i + 1}{\sum_{i=0}^{N} y_i + \sum_{i=0}^{N} p_i + 1}. \tag{3}$$

Pramanik et al. (2024) have demonstrated that hybrid loss functions can effectively improve model performance. Accordingly, we combine Eqs. (2) and (3) to construct a hybrid loss function for training the main fault identification task in the RSM model, which is formulated as follows:

$$\mathcal{L}_{\text{main}} = \mathcal{L}_{\text{bce}} + \mathcal{L}_{\text{dice}}. \tag{4}$$

For the auxiliary tasks, we employ a combination of the Mean Squared Error (MSE) and L1 loss as the overall loss function, which is defined as follows:

$$\mathcal{L}_{\text{aux}} = \mathcal{L}_{\text{MSE}} + \mathcal{L}_{\text{L1}}. \tag{5}$$

Finally, the overall loss function of the RSM model is constructed as a weighted combination of the main task loss (Eq. (4)) and the auxiliary task loss (Eq. (5)), which is expressed as follows:

$$\mathcal{L} = \mathcal{L}_{\text{main}} + \alpha\mathcal{L}_{\text{aux}}, \tag{6}$$

where, α denotes the loss weight of the auxiliary task, determined through experiments.

2.3. Precise segmentation model

During the rough segmentation stage, guided by coherence attributes, the RSM is able to stably identify the overall spatial distribution of faults, providing a reliable structural prior for fault geometry. However, its outputs mainly emphasize a stable representation of the global fault distribution rather than fine-grained modeling of local details. Therefore, it is necessary to further introduce a refinement stage that focuses on localized and detailed modeling to achieve accurate characterization of fault spatial structures. Based on this consideration, we construct a Precise Segmentation Model (PSM) in the second stage. The overall model architecture of the PSM remains consistent with that of the RSM, adopting the same encoder–decoder framework, as illustrated in the right half of Fig. 1. Unlike the RSM, which incorporates manually computed coherence attributes, the PSM employs the fault probability volume learned in the first stage as a fault-enhancement attribute. This volume is concatenated with the original seismic data along the channel dimension and jointly fed into the model.

This design enables the model to employ seismic amplitude information while more effectively leveraging the global fault distribution features extracted in the first stage. Guided by the fault-enhancement attribute, the feature learning process becomes more concentrated on fault-neighborhood regions, thereby reducing interference from background areas during fine-scale modeling. Consequently, the PSM performs targeted modeling around the located fault regions, focusing on fault details, local discontinuities, and the continuity of weak-response fault segments, which allows for refined characterization of fault geometry and spatial continuity. The output of the PSM is a refined fault probability volume that represents the precise spatial locations and continuous structural characteristics of faults, serving as the final fault identification result of our method. During training, the PSM is optimized using the same loss function formulation as the RSM. Considering the high consistency between the PSM and RSM in terms of network architecture and task formulation, a transfer learning strategy (Pan and Yang, 2010) is further introduced, in which the parameters of the trained RSM are used to initialize the PSM. This strategy not only significantly accelerates model convergence but also enables effective inheritance of fault-related feature representations learned in the first stage, thereby further improving the accuracy and stability of fault identification in the precise segmentation stage.

2.4. Evaluation metric

For quantitative evaluation of the fault identification results, five commonly used metrics, including Precision, Recall, F1-score, Accuracy, and Intersection over Union (IoU), are employed to assess the overall performance of the model from different perspectives. The corresponding definitions are as follows:

$$P = \frac{\text{TP}}{\text{TP}+\text{FP}}, \tag{7}$$

$$R = \frac{\text{TP}}{\text{TP}+\text{FN}}, \tag{8}$$

$$F1 = 2\frac{P\times R}{P+R}, \tag{9}$$

$$\text{ACC} = \frac{\text{TP}+\text{TN}}{\text{TP}+\text{TN}+\text{FP}+\text{FN}}, \tag{10}$$

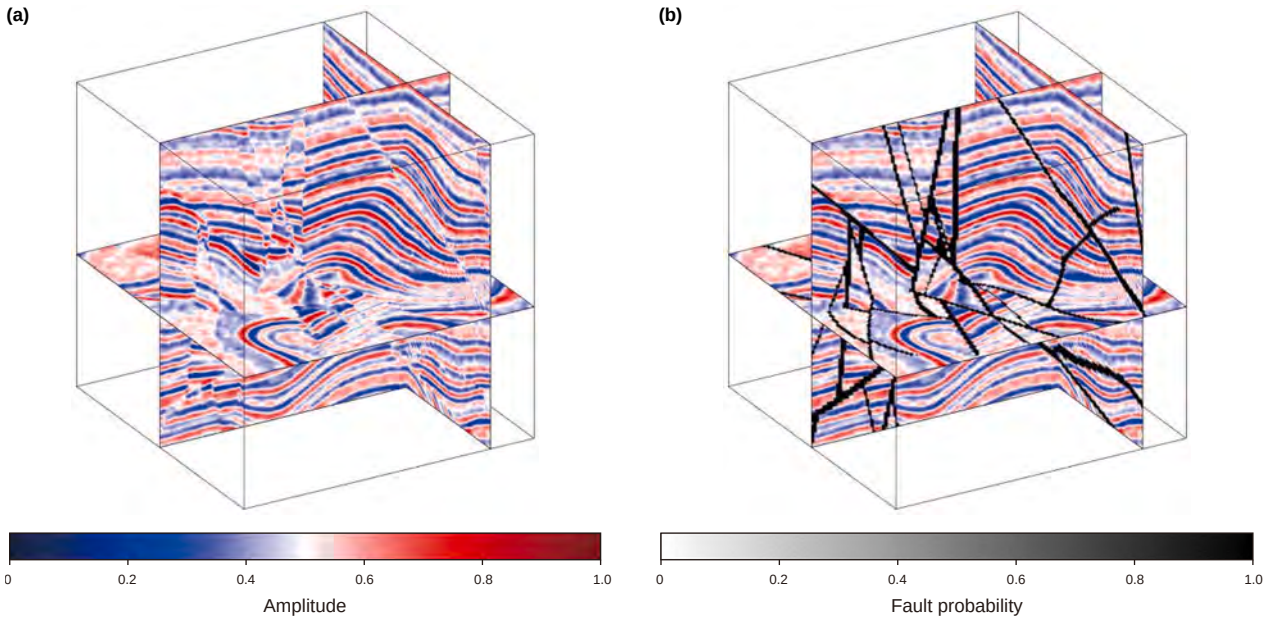


Fig. 3. Synthetic fault data: **(a)** Seismic data, **(b)** fault label.

$$\mathrm{IoU} = \frac{\mathrm{TP}}{\mathrm{TP} + \mathrm{FP} + \mathrm{FN}}, \tag{11}$$

where, TP (True Positive), TN (True Negative), FP (False Positive), and FN (False Negative) denote the numbers of true positives, true negatives, false positives, and false negatives in fault prediction, respectively.

Among these metrics, Precision and Recall are used to evaluate the model's discrimination accuracy and detection capability for faults, respectively, while Accuracy reflects the overall classification accuracy of the model for the seismic data volume. However, in fault identification tasks, fault samples typically constitute only a small fraction of the seismic volume, resulting in a highly imbalanced class distribution. Under such conditions, Accuracy alone may not fully reflect the model's performance. In this context, the F1-score and IoU take both false positives and false negatives into account, providing a more effective measure of overall performance under class imbalance. Therefore, they serve as key metrics for assessing model performance.

3. Experiments

3.1. Data illustration

Obtaining field fault labels is often challenging in practice; as a result, synthetic data are commonly used for model training. Wu et al. (2020) introduce a workflow for generating synthetic fault data. The procedure consists of the following steps: first, a horizontal reflection coefficient model is generated. Next, folds are added to the model. Faults are then incorporated by defining the near-fault displacement field, fault plane, and fault traction factor. Finally, the result is convolved with a wavelet and noise is added to produce synthetic fault data volumes. Based on this workflow, we generate 110 pairs of relatively complex fault data, which are combined with 220 pairs of synthetic data provided by Wu et al. (2019a) to form the training and testing dataset. The combined dataset contains 300 pairs for training and 30 pairs for testing, all with a size of 128 × 128 × 128. A schematic diagram of the synthetic fault data is shown in Fig. 3. For each data volume, standardization and flipping-based data augmentation are applied.

3.2. Implementation details

Our proposed method and the comparative approaches are implemented using the PyTorch framework in Python. All experiments are conducted on a computer equipped with a Quadro RTX 5000 GPU with 16 GB of memory. Model training uses the Adam optimizer with a batch size of 2 and a learning rate of 1e-4. To mitigate overfitting, an early stopping strategy is applied during training: the process terminates if the validation loss does not decrease over 8 consecutive epochs.

During model training, the hybrid loss function defined in Eq. (6) is used. The weight parameter α is determined experimentally. In our work, α is set to 0.2, 0.4, 0.6, and 0.8, and parameter selection is conducted on the test set. Subsequently, the performance of models under different parameter configurations is compared using the evaluation metrics computed from Eqs. (7)–(11). The results are presented in Table 2. The experiments indicate that the overall model performance is optimal when α is set to 0.4; therefore, this configuration is adopted in all subsequent experiments.

Based on the above optimal parameter settings, the single-stage baseline models (UNet3D (Wu et al., 2019a), ResUNet3D (Zhang et al., 2018), Attention UNet3D (Oktay et al., 2018), TransBTS (Wang et al., 2021c), and UNETR (Hatamizadeh et al., 2021)) as well as the proposed two-stage model are trained on the same dataset. Fig. 4 presents the loss convergence curves of all models during training. It can be observed that the training and validation losses of all models gradually decrease and eventually stabilize, indicating that all models have converged and providing a reliable basis for the subsequent comparison of fault identification performance.

Table 2
Test set evaluation metrics under different α values.

α	Precision	Recall	F1	Accuracy	IoU
0.2	0.7696	0.8560	0.8102	0.9708	0.6829
0.4	**0.7806**	**0.8494**	**0.8134**	**0.9713**	**0.6881**
0.6	0.7687	0.8475	0.8060	0.9699	0.6775
0.8	0.7523	0.8601	0.8022	0.9686	0.6727

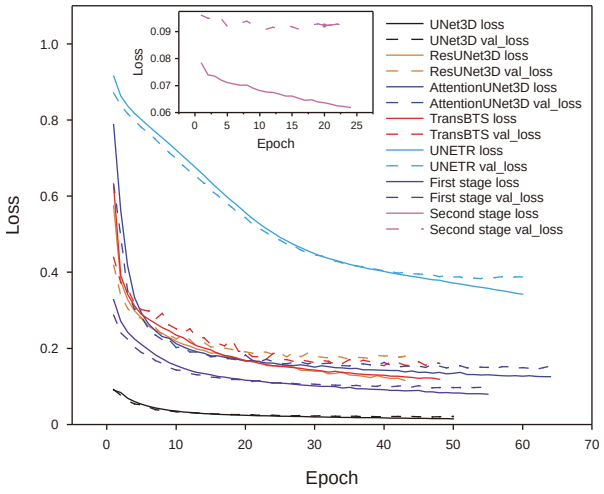


Fig. 4. Convergence curves of the training loss functions for different models.

4. Experimental results

4.1. Synthetic data

To comprehensively assess the performance of the proposed method on synthetic seismic datasets, the proposed two-stage framework is compared with representative single-stage baseline models in terms of computational efficiency, quantitative metrics, and qualitative visual results.

First, the stage-wise recognition performance of the proposed two-stage method is analyzed through the visualization of test data (Fig. 5). The results indicate that the first stage is able to identify the major fault structures and capture the overall spatial distribution of faults. However, its capability in delineating fault intersections and weak-response regions remains limited. In contrast, the second stage further improves the fault recognition accuracy and the representation of fine-scale details. The predicted fault structures exhibit more accurate delineation of intersecting faults and local geometric features, showing a high degree of consistency with the ground-truth labels. These observations demonstrate the effectiveness of the two-stage strategy in enhancing both recognition accuracy and structural detail representation. In addition, the predicted results of the auxiliary task show a high degree of spatial consistency with the corresponding labels, suggesting that the auxiliary task can be effectively learned by the network and may provide complementary information for the main fault recognition task.

Table 3
Comparison of computational efficiency and complexity metrics for different models.

Model	Params, M	FLOPs, G	Inference time, s
UNet3D	1.460	137.435	0.048
ResUNet3D	5.687	509.855	0.112
AttentionUNet3D	24.561	583.975	0.210
TransBTS	32.790	261.325	0.134
UNETR	93.011	195.102	0.086
Our method	2.040 × 2	240.349	0.082 × 2

In terms of computational efficiency and model complexity (Table 3), different models exhibit substantial differences in the number of parameters, FLOPs, and inference time. For the proposed two-stage method, since rough segmentation and precise segmentation are performed sequentially, the overall computational cost is approximately twice that of its single-stage counterpart; this is explicitly indicated as " × 2" in Table 3. UNet3D exhibits the smallest number of parameters and the lowest FLOPs, resulting in minimal computational overhead. ResUNet3D, despite having a moderate parameter count, exhibits a significant increase in FLOPs, reflecting the higher computational cost introduced by residual structures in three-dimensional scenarios. Attention UNet3D further increases both parameter count and FLOPs due to the incorporation of attention mechanisms, leading to a corresponding increase in inference time. For the Transformer-based model UNETR, although it has the largest parameter scale (93.011 M), its FLOPs do not increase proportionally, indicating that the computational burden is mainly associated with high-dimensional feature representations and self-attention modeling processes. TransBTS exhibits intermediate parameter and FLOPs values between conventional CNN-based models and UNETR, reflecting the trade-off characteristics of hybrid architectures. By contrast, the proposed two-stage method contains only 2.040 M parameters and 240.349G/128^3 FLOPs in the single-stage setting. Even when considering the sequential inference of the two stages, its overall parameter scale remains substantially smaller than that of models employing complex attention mechanisms or Transformer architectures, while the computational complexity remains manageable. Consequently, the inference time is comparable to that of more complex models, demonstrating a favorable balance between structural complexity and computational efficiency.

In the quantitative evaluation results (Table 4), it can be observed that there are significant differences in the performance of different models across various indicators. Overall, single-stage models with larger parameter scales and higher architectural complexity, such as ResUNet3D, Attention UNet3D, and TransBTS, achieve relatively superior performance in terms of Precision, F1-

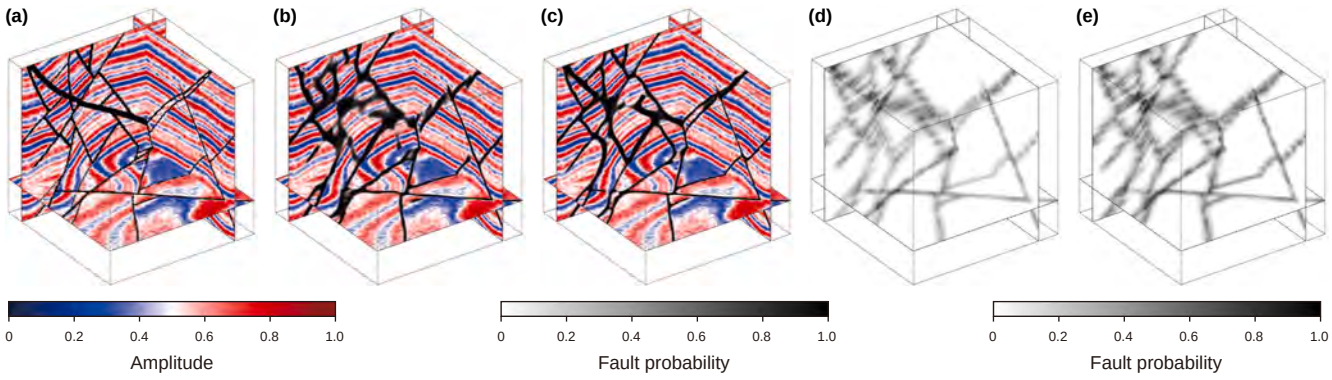


Fig. 5. Visualization of stage-wise fault recognition results obtained from the proposed two-stage method on the test set: **(a)** Seismic data with the corresponding ground-truth labels, **(b)** Recognition results of the first stage, **(c)** Recognition results of the second stage, **(d)** Ground-truth labels of the auxiliary task, **(e)** Predicted results of the auxiliary task.

Table 4
Quantitative performance comparison of different models on the test set.

Model	Precision	Recall	F1	Accuracy	IoU
UNet3D	0.5559	**0.9580**	0.7028	0.9404	0.5430
ResUNet3D	0.8351	0.8982	0.8654	0.9794	0.7641
AttentionUNet3D	0.8506	0.9085	**0.8785**	0.9813	**0.7847**
TransBTS	**0.8544**	0.9022	0.8775	**0.9815**	0.7828
UNETR	0.6674	0.7604	0.7073	0.9547	0.5504
Our method	0.7806	0.8494	0.8134	0.9713	0.6881

score, and IoU. This indicates that, under synthetic data conditions, increased model capacity is beneficial for learning the regular geometric patterns and well-defined boundaries of fault structures. It is worth noting that although UNETR has the largest parameter size among all the methods, its overall quantitative performance is not competitive. Specifically, its F1-score and IoU are markedly lower than those of several convolution-based models. This suggests that relying solely on global self-attention mechanisms does not necessarily yield performance gains for fault identification tasks, particularly in scenarios where local discontinuous structures dominate, as the modeling of fine-scale geometric details remains limited. The proposed two-stage method does not achieve the highest absolute values on the synthetic dataset; however, it attains a more balanced trade-off between Precision and Recall, and demonstrates stable and consistent improvements in comprehensive metrics such as F1-score and IoU. Compared with the baseline UNet3D, a substantial enhancement in overall recognition performance is observed. Meanwhile, its performance remains comparable to that of more complex single-stage models, highlighting the effectiveness and robustness of the two-stage strategy under synthetic data conditions.

The visualization results (Fig. 6) indicate that all models are capable of effectively identifying the overall strike and geometric characteristics of faults. From a comparative perspective, UNet3D, as a basic convolutional model, produces relatively rough identification results. Its fault response regions exhibit noticeable blurring, with insufficiently clear local fault boundaries, and limited capability in delineating small-scale structures and weak faults. This suggests that the basic simple CNN model has certain limitations in capturing fine fault details. The results obtained by UNETR are generally consistent with the ground truth in terms of the overall fault trend, and can correctly reflect the macroscopic spatial trend of the faults. However, its faults tend to appear as scattered or discontinuous points, making it difficult to form continuous band-like structures, which leads to relatively poor spatial continuity. This phenomenon indicates that global self-attention–based modeling is advantageous for capturing large-scale fault trends, but remains limited in representing local continuity and elongated fault structures. In contrast, single-stage models such as ResUNet3D, Attention UNet3D, and TransBTS are able to more accurately characterize the spatial morphology of faults. Their results exhibit clearer fault boundaries and more refined local geometric details. In regions where faults are relatively continuous, these models can produce coherent fault representations that are highly consistent with the ground truth. This improvement can be attributed to deeper network architectures and the incorporation of attention mechanisms or global modeling strategies, which enhance feature representation capacity on synthetic datasets. The proposed two-stage method yields visualization results on synthetic data that are overall comparable to those of these more complex models. It can stably identify the main fault structures while maintaining good spatial continuity and structural consistency. Although its level of detail in certain local regions may not always exceed that of large-parameter single-stage models, the fault results obtained by the proposed method exhibit a more uniform spatial distribution, without noticeable scattered noise or structural fragmentation.

The combined quantitative and visual results show that under the synthetic data conditions, all models are capable of effectively

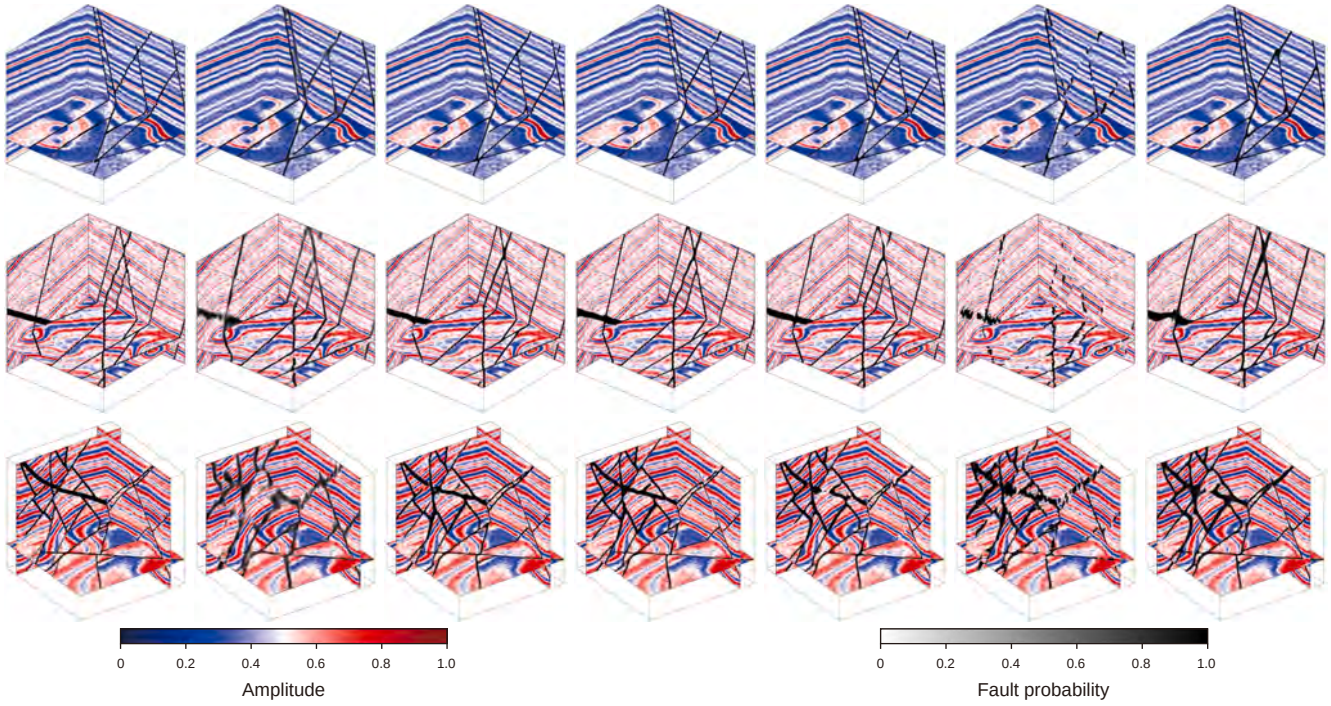


Fig. 6. Visualization comparison of fault recognition results of different models on the test set: From left to right: seismic data with corresponding ground-truth labels, UNet3D, ResUNet3D, Attention UNet3D, TransBTS, UNETR, and the proposed method.

identifying the overall fault structures. The increase in model complexity mainly manifests in the enhancement of local details, while the improvement in the overall fault identification performance is relatively limited. It should be noted that the fault structures in synthetic datasets are relatively idealized and subject to limited noise interference, resulting in relatively small performance differences among different models. In contrast, fault geometries in field seismic data are more complex and are significantly affected by noise and geological heterogeneity. Under such conditions, the differences in robustness and structural modeling capability among various methods are expected to become more pronounced. Therefore, it is necessary to further evaluate and compare the proposed method with other approaches on field seismic data.

4.2. Field seismic data

After validating the effectiveness of the proposed method on synthetic data, it is further necessary to evaluate its practical applicability and stability on field seismic data. Specifically, comparative experiments are conducted on three field seismic data with distinct geological settings and data characteristics, where the proposed method is compared with several representative single-stage fault recognition models. Given the difficulty of obtaining reliable pixel-level fault labels in field seismic data, a qualitative visual comparison is adopted to assess the recognition results of different methods in terms of fault spatial continuity and structural integrity.

4.2.1. Data from offshore western Costa Rica

This seismic data comes from offshore western Costa Rica. As reported in reference (Bangs et al., 2016), this area is characterized by well-developed faults with dense distributions and complex spatial structures. Figs. 7 and 8 present the 3D fault identification results and corresponding local detail comparisons obtained by different methods on this seismic data. In particular, Fig. 8 additionally includes the manually interpreted fault results as a reference, which facilitates a comparative analysis of the performance of different methods in terms of fault location, orientation, and continuity. From the visualization results, it can be observed that the fault recognition performance varies noticeably among different models, reflecting varying adaptability of different model architectures under complex geological conditions. UNet3D is able to identify a certain number of fault structures, but its results are generally diffuse, with relatively blurred fault boundaries and local spreading effects, making it difficult to form stable and continuous fault representations. The recognition performance of ResUNet3D and TransBTS degrades on this seismic data, with only sporadic faults detected in limited areas and a lack of coherent fault structures. Attention UNet3D shows slight improvement over the aforementioned models by capturing local fault structures in some regions, but the overall fault continuity and spatial completeness remain limited. The fault results produced by UNETR are generally consistent with the overall geological trends; however, they tend to appear as sparsely distributed points rather than continuous band-like structures, indicating limitations in modeling local geometric continuity in field seismic data. By contrast, the proposed two-stage method is able to identify more continuous and coherent fault structures on this dataset, with a spatial distribution exhibiting good overall consistency. By comparing the results with the manual interpretations, it can be observed that the major faults identified by the proposed method show a high degree of consistency with the manual interpretations in terms of spatial location, overall orientation, and extension trends, demonstrating its effectiveness in extracting fault structures that are consistent with geological understanding. Overall, these observations suggest that some single-stage models that perform well on synthetic datasets experience a certain degree of performance degradation in the synthetic-to-field scenario, whereas the proposed two-stage method demonstrates more stable structural consistency and spatial continuity on field seismic data. Moreover, its results exhibit good correspondence with manual interpretations at the local detail level, indicating strong potential for practical field applications.

4.2.2. Land seismic data

This seismic data originates from a land survey, where the fault structures are relatively well-defined. Compared with the previous field data, this dataset exhibits lower noise interference and more distinct fault geometric features. Figs. 9 and 10 present the 3D fault identification results and local detail comparisons obtained by different methods on this seismic data. In Fig. 10, the manually interpreted faults are also provided as a reference to facilitate a comparative evaluation of different methods in terms of fault location, orientation, and continuity. Overall, the recognition performance of all models shows an overall improvement relative to the previous field data, although differences among model performances remain observable. UNet3D is able to detect a larger number of fault structures, but the predictions exhibit relatively blurred boundaries and limited local continuity. ResUNet3D and TransBTS detect some major faults; however, their results appear fragmented, which makes it difficult to form coherent fault structures. Attention UNet3D and UNETR primarily produce discontinuous or scattered fault predictions, indicating that capturing local geometric continuity remains relatively limited. In comparison, the proposed two-stage method demonstrates relatively stable identification of fault structures with better spatial continuity. Its predictions show clearer fault outlines, more consistent overall structures, and improved continuity in weak-response regions. Compared with the manual interpretations, it can be observed that although certain discrepancies remain in local details, the identified major faults are generally consistent with the manual interpretations in terms of spatial location and overall distribution patterns. This indicates that the proposed method can reliably extract fault structures that are consistent with geological understanding. These results demonstrate that single-stage methods may still face limitations in maintaining fault continuity and structural integrity, whereas the rough-to-precise two-stage strategy can provide enhanced stability and reliability in fault identification.

4.2.3. Data from Western Australia

This seismic data comes from Western Australia. Compared with the previous two datasets, the fault structures in this dataset are more complex, featuring intersections, branching, and superposition, which places higher demands on the models' spatial representation capability and robustness. Figs. 11 and 12 present the 3D fault identification results and local detail comparisons of different methods on this field seismic data. In particular, Fig. 12 also includes the manually interpreted faults as a reference, enabling a comparative evaluation of different methods in terms of their ability to characterize fault spatial location, geometric morphology, and continuity in complex fault zones. In this complex fault scenario, the performance of single-stage models generally decreases. UNet3D is able to detect a certain number of fault structures, but its predictions exhibit limitations in boundary clarity and local continuity, making it challenging to fully capture the overall geometry of the complex fault system. ResUNet3D and TransBTS show relatively limited detection capability on this dataset, identifying only isolated fault segments in certain regions,

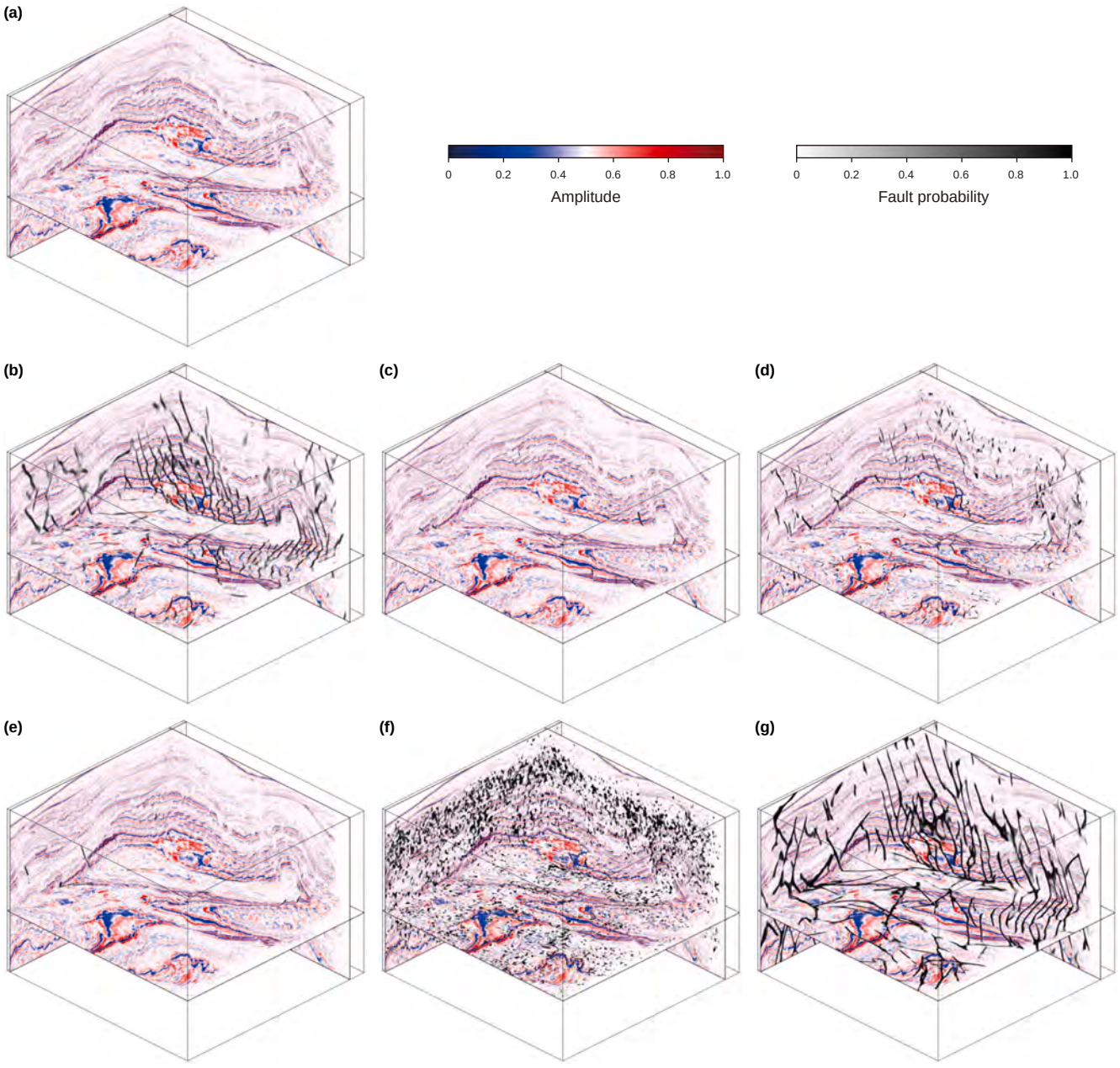


Fig. 7. Comparison of three-dimensional fault identification results of different methods on offshore western Costa Rica seismic data: **(a)** Seismic data, **(b)** The identification results of the UNet3D, **(c)** The identification results of the ResUNet3D, **(d)** The identification results of the Attention UNet3D, **(e)** The identification results of the TransBTS, **(f)** The identification results of the UNETR, **(g)** The identification results of the proposed method.

and failing to form a stable and coherent fault distribution. Attention UNet3D demonstrates some improvement compared with the previous two models, detecting a larger number of local faults; however, the overall results are still dominated by discontinuous or fragmented fault segments, and complete, continuous fault systems are difficult to reconstruct in regions with intersecting faults. UNETR can reflect the general trend of faults in local regions, but its predictions are primarily sparse and point-like, and fail to form continuous, strip-like fault structures in areas with intersecting or multi-branch faults. In contrast, the proposed two-stage fault identification method is capable of stably detecting richer and more continuous fault structures on this complex dataset. Its predictions maintain good spatial continuity and overall consistency even in areas with fault intersections and branches, providing a relatively complete representation of the geometric characteristics of the fault system. By comparison with the manual interpretations, it can be observed that although certain discrepancies remain in some local details, the faults identified by the proposed method are generally consistent with the manual interpretations in terms of spatial location and overall geometric morphology. These results indicate that, in field seismic data with complex fault structures, single-stage end-to-end models may exhibit limited performance, whereas the proposed method, guided by stage-wise prior modeling, maintains stable fault identification performance, further demonstrating its robustness and applicability in complex field scenarios.

The comprehensive results of fault identification across the three field seismic datasets indicate that, as the complexity of

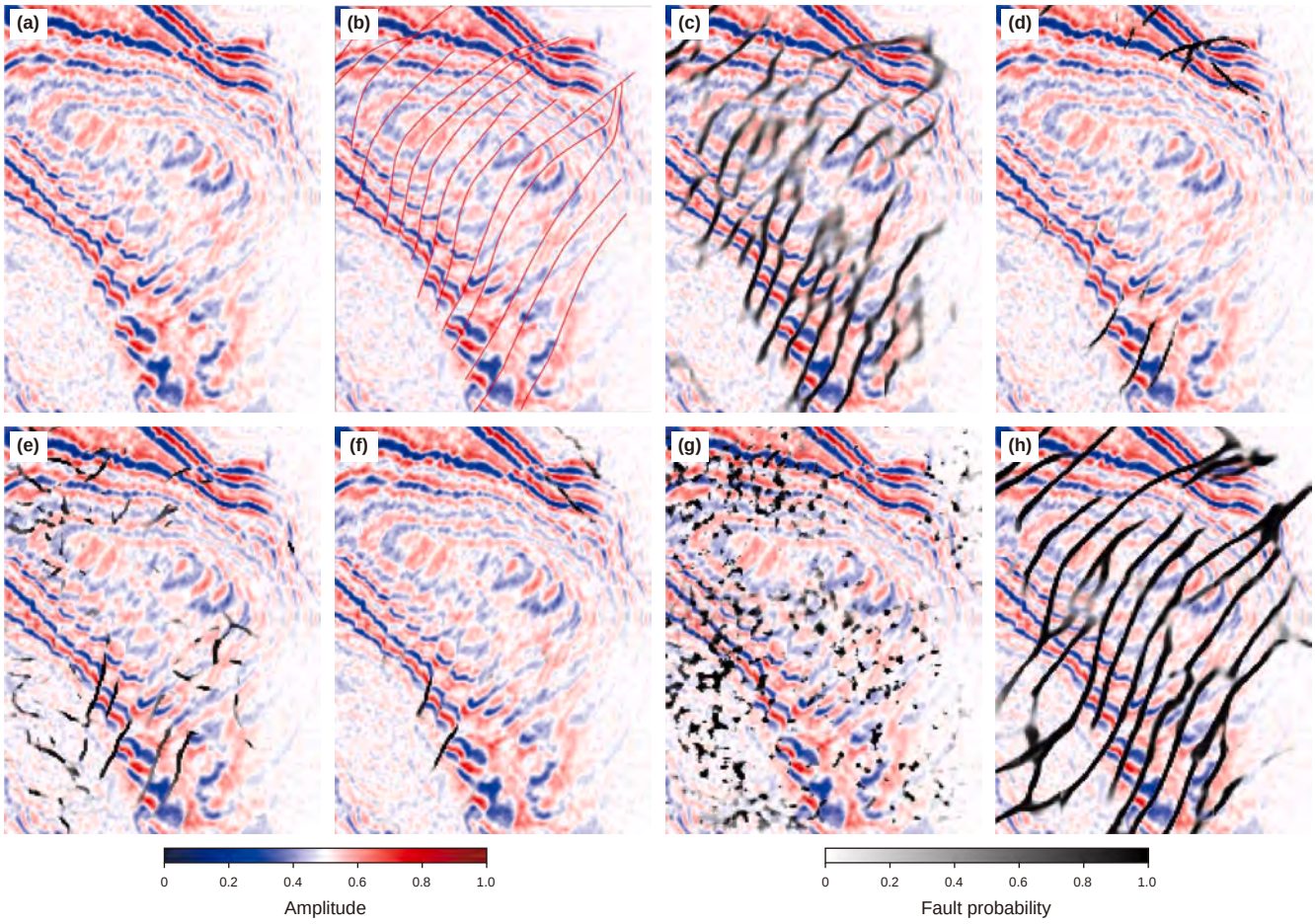


Fig. 8. Comparison of local fault identification details of different methods on offshore western Costa Rica seismic data: **(a)** Seismic data, **(b)** Manual interpretations, **(c)** The identification results of the UNet3D, **(d)** The identification results of the ResUNet3D, **(e)** The identification results of the Attention UNet3D, **(f)** The identification results of the TransBTS, **(g)** The identification results of the UNETR, **(h)** The identification results of the proposed method.

geological structures increases, the performance of the comparison methods on field data exhibits varying degrees of deterioration. For datasets with relatively clear fault structures, most models are able to capture the main fault trends reasonably well, yet limitations remain in terms of boundary clarity, spatial continuity, and local structural completeness. In scenarios with dense faults or more complex configurations such as intersections and branching, the identification results tend to appear fragmented, discontinuous, or scattered, making it difficult to form a complete and continuous fault system. By contrast, the proposed two-stage method demonstrates stable and consistent performance across datasets with varying structural complexity, maintaining relatively continuous and structurally coherent fault representations in complex regions, thereby exhibiting good robustness and potential for practical application.

4.3. Ablation experiments

We propose a two-stage fault identification method guided by coherence attribute priors. To systematically evaluate the effectiveness of each key component, targeted ablation experiments are conducted on both synthetic data and field seismic data from Western Australia. Under the condition that the overall network architecture and training strategy remain unchanged, specific modules are sequentially removed or replaced to analyze their impact on fault identification performance. Specifically, three sets of ablation experiments are designed. First, to assess the contribution of coherence attributes as prior inputs, a comparison is performed between models with and without coherence attribute inputs. In this experiment, the two-stage framework is maintained, and only the C3 coherence attribute input is removed in the first stage to evaluate its contribution on the model's performance. Second, to validate the rationality of the proposed two-stage modeling strategy, a comparison is conducted between a single-stage method and the two-stage method. The single-stage method directly uses the output of the first-stage model as the final fault identification result. By comparing it with the complete two-stage method, the effectiveness of reconstructing the fault identification process from a single end-to-end stage to a rough-to-precise two-stage workflow is demonstrated. Finally, to examine the effectiveness of the auxiliary task constructed from local data around faults, a comparison is made with a model using data reconstruction as the auxiliary task. In this experiment, the two-stage backbone remains unchanged, and only the auxiliary task labels are replaced: the reconstruction task uses the original seismic data as the target, whereas the proposed auxiliary task uses specifically designed labels, allowing the evaluation of how different auxiliary task designs affect the performance of the main fault identification task.

The quantitative results of the aforementioned ablation experiments on the test set are presented in Table 5. First, comparing the “Without coherence attributes” setting with our method

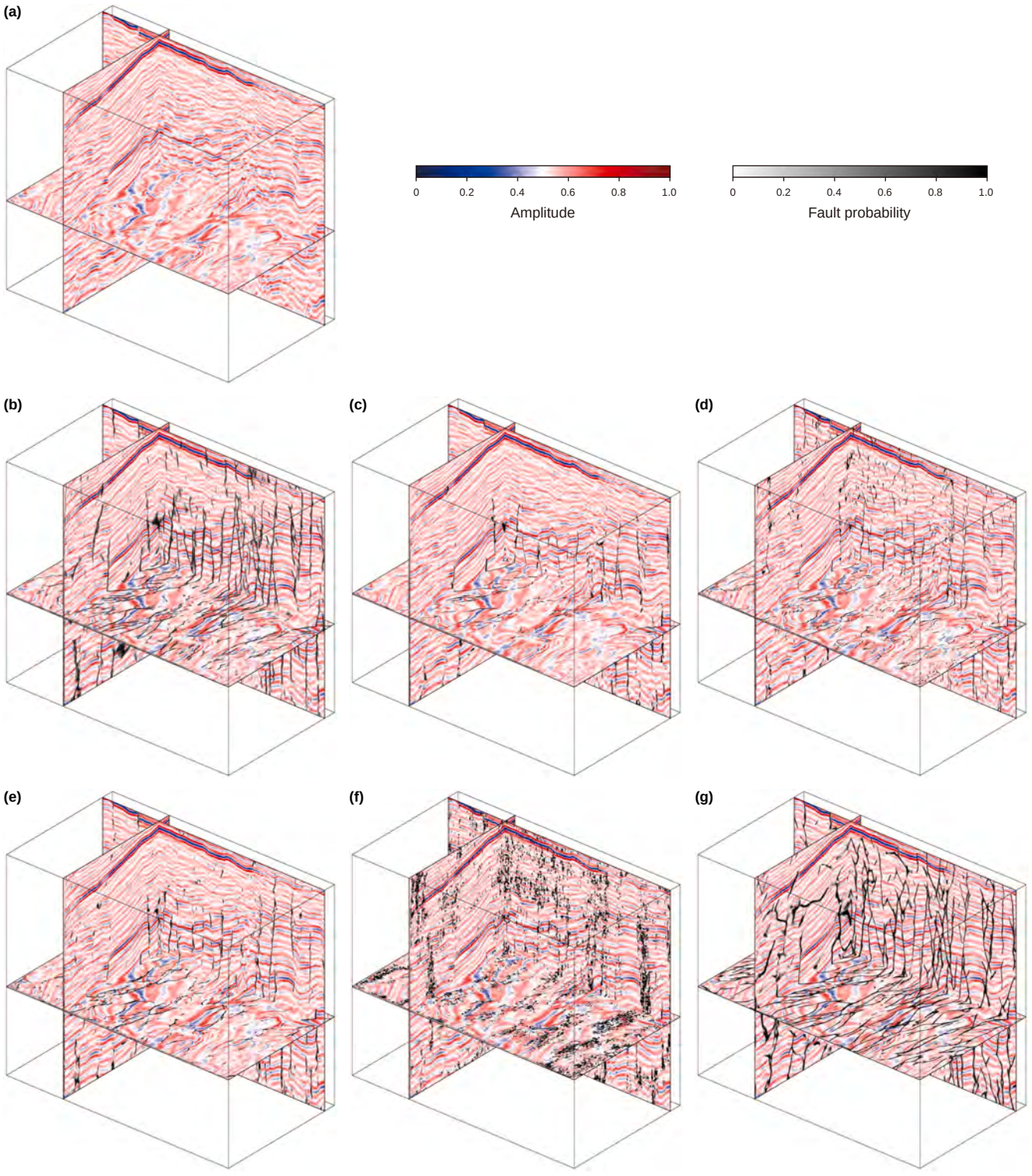


Fig. 9. Comparison of three-dimensional fault identification results of different methods on field seismic data from a land survey: **(a)** Seismic data, **(b)** The identification results of the UNet3D, **(c)** The identification results of the ResUNet3D, **(d)** The identification results of the Attention UNet3D, **(e)** The identification results of the TransBTS, **(f)** The identification results of the UNETR, **(g)** The identification results of the proposed method.

shows that incorporating coherence information yields certain improvements in Precision, F1, and IoU. This indicates that coherence, as a prior highlighting discontinuous structures in seismic data, facilitates more accurate localization of fault regions while effectively suppressing false detections in background areas, thereby enhancing the overall quality of fault identification. It can also be observed that the model achieves a higher recall under the "Without coherence attributes" setting. This may be attributed to the absence of prior information provided by coherence attributes, which makes the model more prone to over-prediction. As a result, more potential fault regions are identified as faults, leading to fewer false negatives. However, such over-prediction also

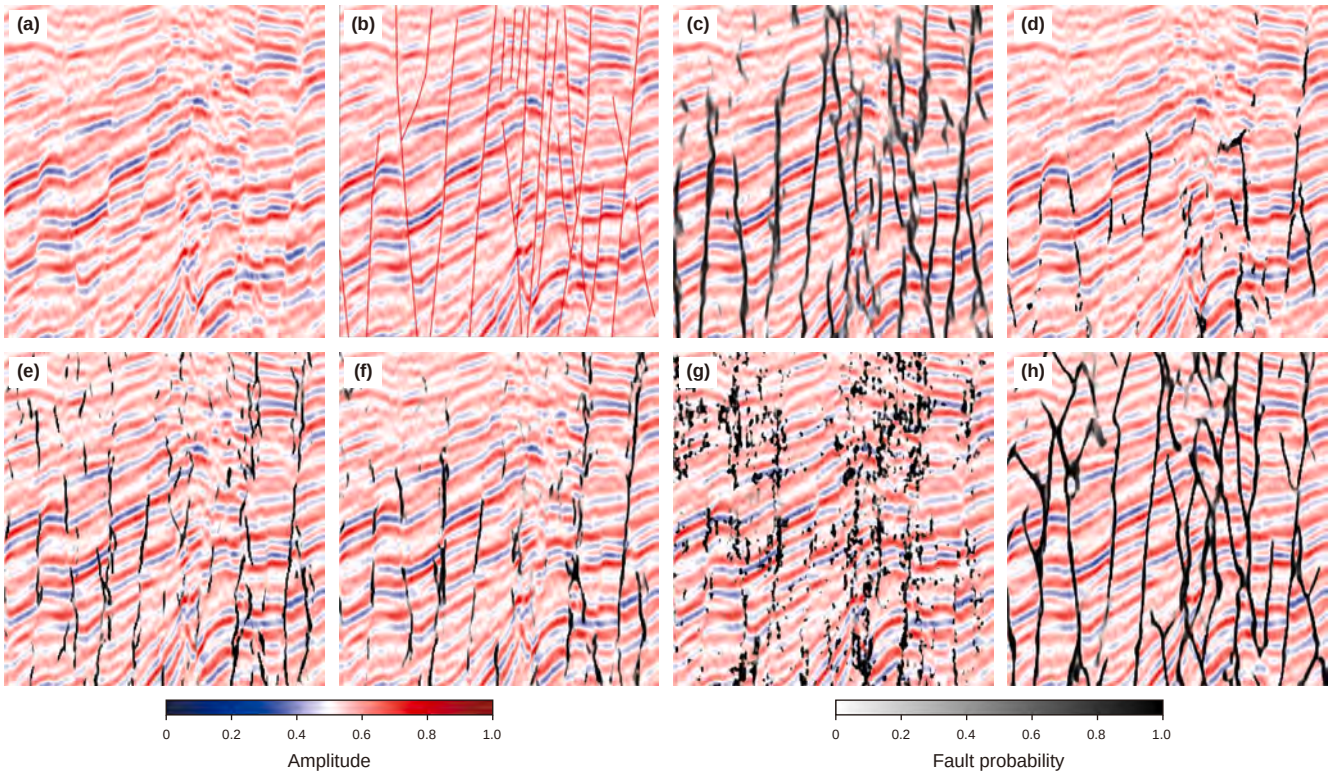


Fig. 10. Comparison of local fault identification details of different methods on field seismic data from a land survey: **(a)** Seismic data, **(b)** Manual interpretations, **(c)** The identification results of the UNet3D, **(d)** The identification results of the ResUNet3D, **(e)** The identification results of the Attention UNet3D, **(f)** The identification results of the TransBTS, **(g)** The identification results of the UNETR, **(h)** The identification results of the proposed method.

introduces a larger number of false positives, thereby degrading performance in terms of Precision and IoU. In contrast, when coherence attributes are incorporated, the model is guided by fault-related structural priors, enabling more accurate fault predictions. This effectively reduces false positives and improves the reliability of the detection results. Second, the comparison between the single-stage and two-stage methods demonstrates that the two-stage approach achieves superior performance in the F1 and IoU metrics. This suggests that decomposing the fault identification process into a "rough-to-precise" two-stage framework helps to further improve the overall quality and stability of the results based on the preliminary identification of fault distributions. Finally, compared with using data reconstruction as an auxiliary task, the proposed auxiliary task based on local fault-neighborhood data shows certain advantages in Precision, F1, and IoU, indicating that this auxiliary task can more effectively provide a collaborative constraint with the main fault identification task, thereby enhancing the model's discriminative capability for fault structural features.

The visualization results of the ablation experiments on the Western Australia seismic data are shown in Fig. 13. Fig. 13(a) presents the results without the incorporation of coherence attributes, Fig. 13(b) shows the results of the single-stage method, Fig. 13(c) corresponds to the results using data reconstruction as the auxiliary task, and Fig. 13(d) illustrates the results of the proposed method. Comparing Fig. 13(a) and (d), it is observed that without coherence attributes, the number of identified faults is limited and the continuity is poor, making it difficult to accurately capture the overall orientation and spatial distribution of the fault structures; the introduction of coherence attributes leads to improvements in fault quantity, continuity, and spatial consistency (as shown in the green boxes). Further comparison between Fig. 13(b) and (d) indicates that while the single-stage method detects some faults, the overall continuity and structural integrity remain insufficient, whereas the two-stage method achieves more stable and coherent fault distributions (as shown in the purple boxes), validating the effectiveness of the staged modeling strategy under complex field scenarios. Finally, comparison of Fig. 13(c) and (d) demonstrates that the proposed auxiliary task, constructed based on local fault-neighborhood data, better enhances the continuity of fault details and captures weakly responsive regions, indicating that the designed auxiliary task positively contributes to improving fault identification quality in field seismic data.

In summary, both the quantitative analysis on synthetic data and the qualitative visualization on field seismic data demonstrate that the key modules of the proposed two-stage method guided by coherence attribute priors contribute positively to enhancing fault recognition performance, enabling the model to achieve improved overall performance in terms of fault spatial continuity, structural consistency, and applicability to field seismic data.

5. Discussion

The proposed two-stage fault recognition framework decomposes the task into two functionally distinct stages: "rough localization" and "precise characterization," aiming to alleviate structural instability and noise interference commonly observed in single-stage end-to-end methods applied to complex seismic data. The first stage focuses on generating a stable representation of the overall fault spatial distribution, providing spatially consistent structural guidance for subsequent identification. Building upon this, the second stage concentrates on fault-related regions, enhancing geometric continuity and local detail modeling to achieve more refined fault delineation. Experimental

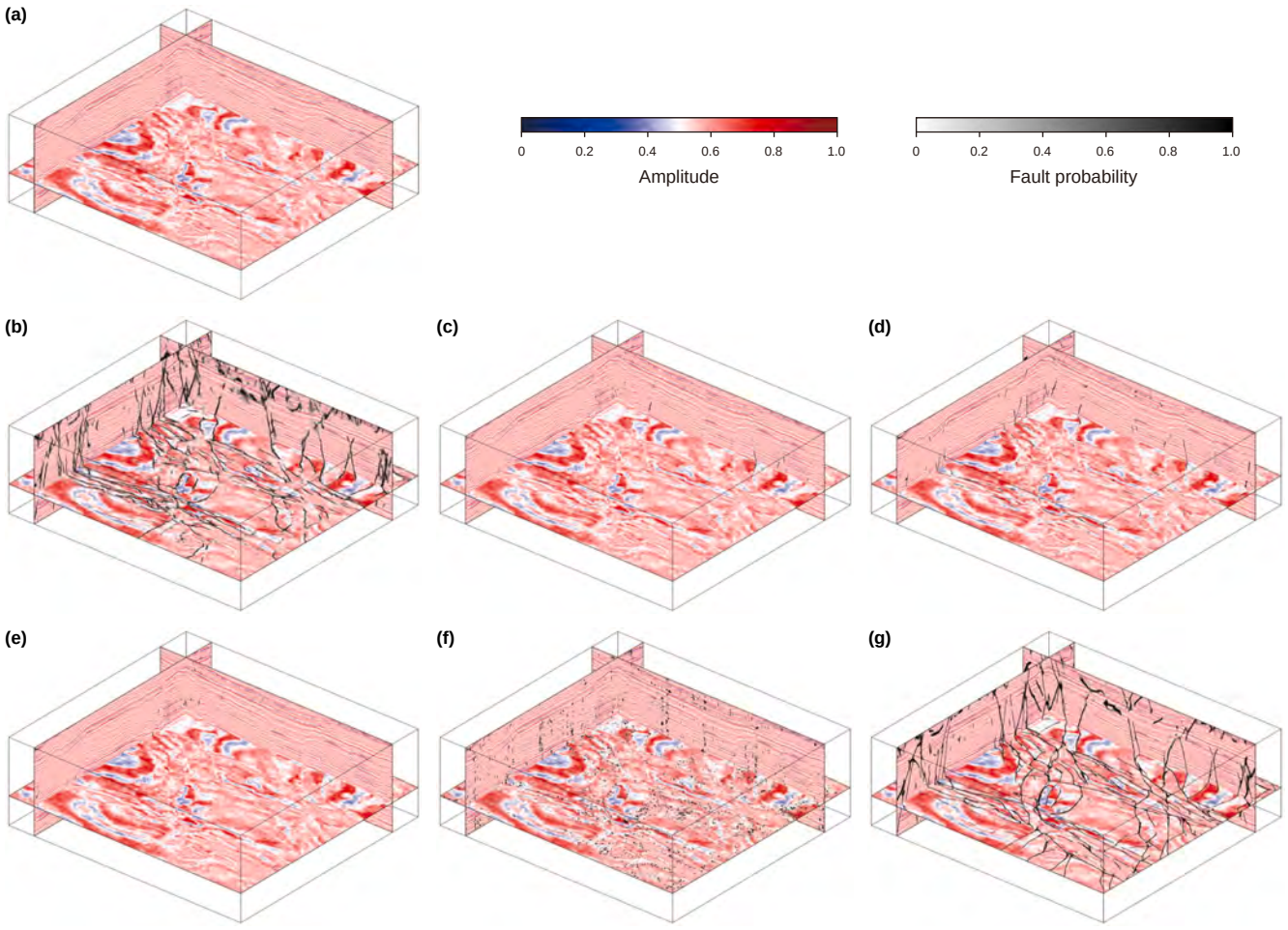


Fig. 11. Comparison of three-dimensional fault identification results of different methods on western Australia seismic data: **(a)** Seismic data, **(b)** The identification results of the UNet3D, **(c)** The identification results of the ResUNet3D, **(d)** The identification results of the Attention UNet3D, **(e)** The identification results of the TransBTS, **(f)** The identification results of the UNETR, **(g)** The identification results of the proposed method.

results indicate that this two-stage strategy yields more stable identification performance on both synthetic and field seismic data. In field data, the first-stage output captures the general fault distribution but exhibits limitations in continuity and weak-response areas; incorporating the second stage produces more spatially coherent results, confirming the effectiveness of the staged modeling in progressively focusing on fault structures under complex geological conditions. It should be noted that the two-stage approach does not merely iteratively refine predictions. The two stages are explicitly distinguished in terms of modeling objectives and prior information: the first stage emphasizes the overall structural stability of faults, whereas the second stage aims to improve geometric consistency and continuity within fault-related regions. Prior information is transmitted between stages in different forms, guiding the model to focus on distinct structural features at each stage rather than repeatedly iterating over the previous-stage outputs, which fundamentally differentiates it from conventional iterative approaches. Specifically, the first stage employs manually computed C3 coherence as a structural prior to enhance the model's perception of discontinuities in seismic data, while the second stage combines the first-stage fault probability volume with the original seismic data, enabling the network to leverage complete amplitude information while concentrating on potential fault regions and suppressing background interference.

In recent years, multi-stage and multi-task learning strategies have been introduced into fault recognition research. For instance, Gao (2024) propose an iterative multi-task learning framework, where the prediction results of the previous round are fed back to the model input for multiple rounds of iteration to optimize fault identification, while Wu et al. (2023) employ seismic data reconstruction as an auxiliary task to enhance the model's fault recognition capability. Although these approaches incorporate multi-stage or multi-task concepts in form, they fundamentally differ from our proposed method in modeling philosophy and information flow design. The method proposed by Gao (2024) relies on prediction-driven iterative refinement, whereas the proposed two-stage framework leverages functional division between stages and distinct forms of prior guidance, progressively transitioning from global fault spatial representation to local geometric characterization without iterative feedback. In contrast to the global reconstruction auxiliary task adopted by Wu et al. (2023), we design an auxiliary task based on local data in the fault neighborhood, guided by the physical characteristics of faults, ensuring high spatial consistency with the main fault recognition task and effectively enhancing the model's ability to discriminate fault structures. Overall, the proposed two-stage strategy is specifically designed for fault recognition in terms of prior forms, stage functionality, and inter-stage information transfer,

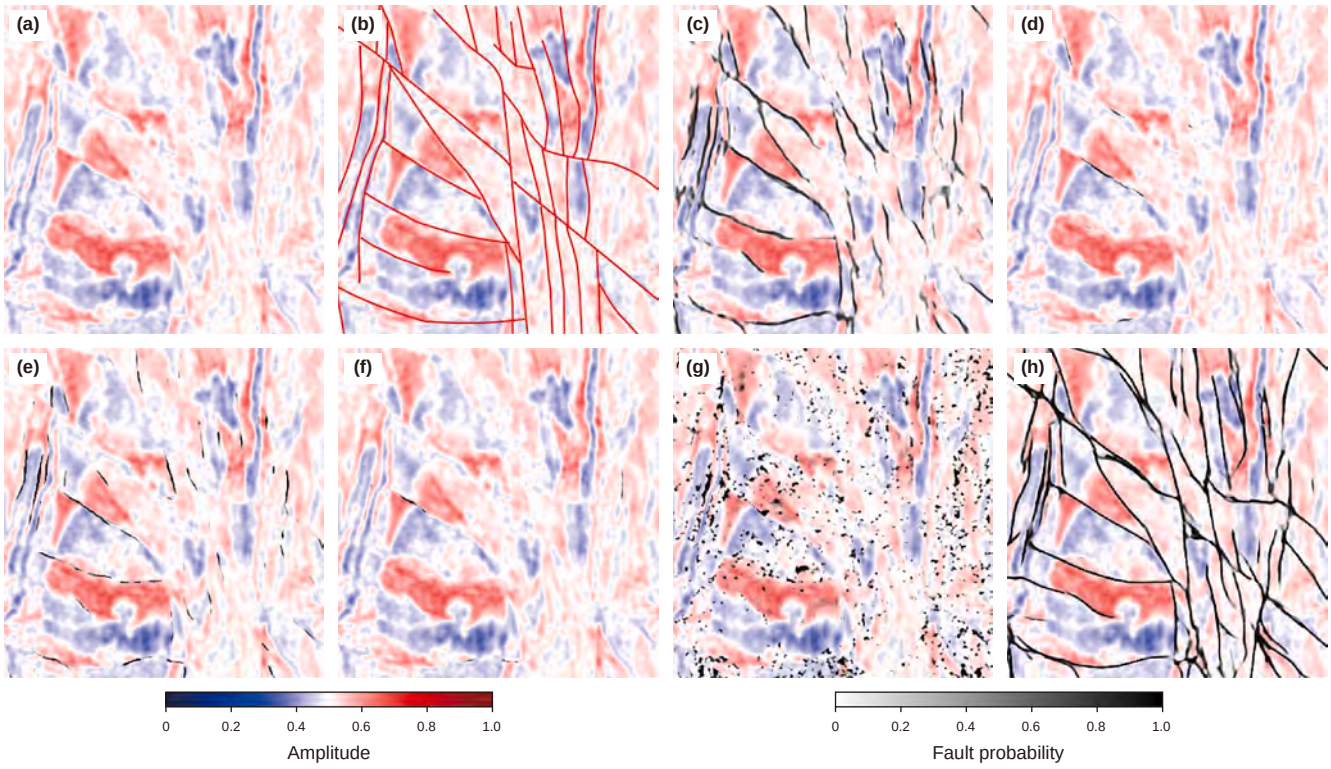


Fig. 12. Comparison of local fault identification details of different methods on western Australia seismic data: **(a)** Seismic data, **(b)** Manual interpretations, **(c)** The identification results of the UNet3D, **(d)** The identification results of the ResUNet3D, **(e)** The identification results of the Attention UNet3D, **(f)** The identification results of the TransBTS, **(g)** The identification results of the UNETR, **(h)** The identification results of the proposed method.

Table 5
Quantitative comparison of ablation experiments on the test set.

Configuration	Precision	Recall	F1	Accuracy	IoU
Without coherence attributes	0.6800	0.9575	0.7947	0.9636	0.6604
Single-stage	0.7406	0.8610	0.7960	0.9674	0.6639
Auxiliary task with data reconstruction	0.7641	0.8669	0.8123	0.9697	0.6858
Our method	0.7806	0.8494	0.8134	0.9713	0.6881

enabling more stable fault identification in complex seismic data while maintaining spatial continuity and structural consistency of faults.

Experimental results demonstrate that several comparative models achieve high quantitative performance on synthetic test datasets, with some models even outperforming the proposed method in metrics such as Precision or F1-score. However, when directly applied to field seismic data, these models often produce fragmented, spatially discontinuous, or even nearly indistinguishable fault predictions, accompanied by performance degradation. This phenomenon primarily arises from the significant data distribution discrepancy between synthetic and field seismic data. Synthetic data are typically characterized by low noise levels, clear fault geometries, and relatively regular structural patterns, which allow high-capacity models with large numbers of parameters to adequately fit idealized fault features. As a result, such models

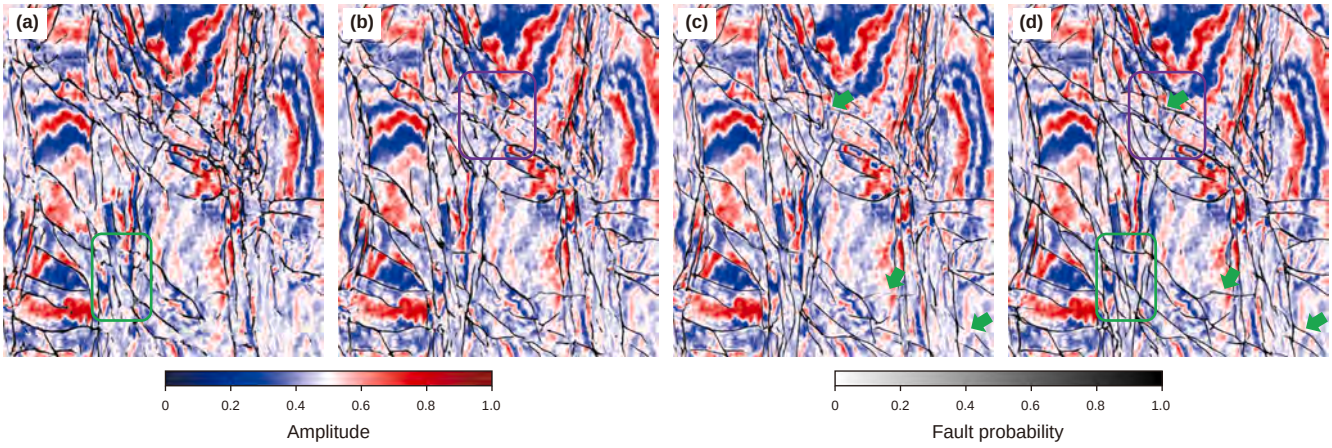


Fig. 13. Visual comparison of fault recognition results for different ablation configurations: **(a)** Results without coherence attributes, **(b)** Single-stage fault recognition results, **(c)** Results with data reconstruction as an auxiliary task, **(d)** Results of the proposed method.

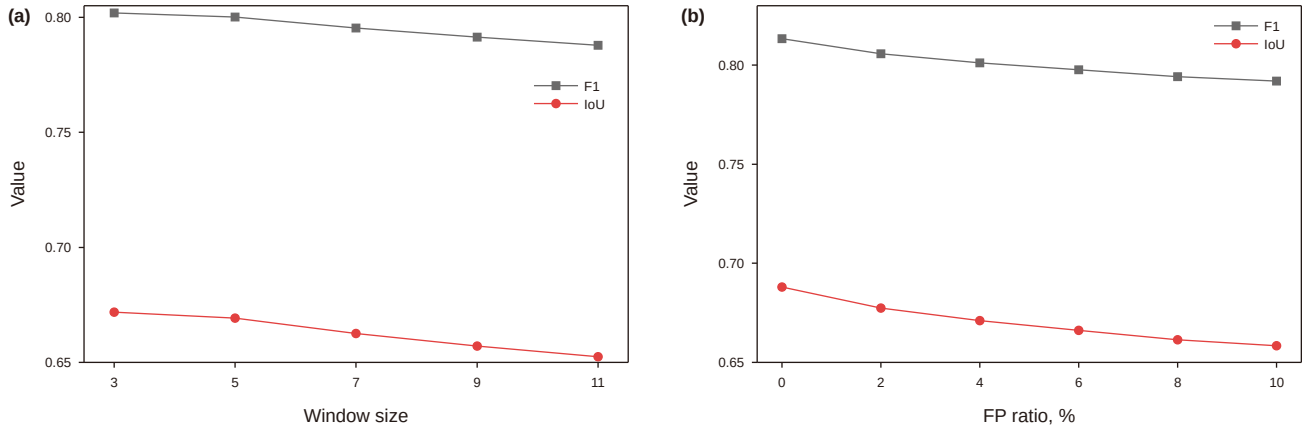


Fig. 14. Performance metric variations in the sensitivity analysis: **(a)** Performance metrics under different C3 coherence attribute calculation window sizes, **(b)** Performance metrics under different FP injection ratios.

tend to learn decision patterns that are highly dependent on the synthetic data distribution, thereby achieving high quantitative performance on synthetic test sets that follow the same distribution as the training data. In contrast, faults in field seismic data usually exhibit more complex and variable geometries, stronger noise interference, and pronounced stratigraphic heterogeneity, and often appear as weak and irregular spatial responses. In the absence of effective structural constraints and prior guidance, single-stage high-capacity models struggle to adapt to these characteristics, resulting in degraded generalization performance in field scenarios. The proposed method alleviates these limitations by introducing fault-related prior information and adopting a stage-wise modeling strategy. Specifically, by incorporating coherence attributes and fault probability–guided information, the model is endowed with fault-related structural constraints that guide feature learning toward spatial and geometric characteristics intrinsic to faults. This prior-guided representation reduces excessive reliance on amplitude information in synthetic-to-field scenarios, thereby enhancing the stability and applicability of the model on field seismic data. Therefore, the proposed method is more suitable for synthetic-to-field scenarios where there exists a significant distribution gap between synthetic and field seismic data, particularly in cases with strong noise interference, weak fault responses, and complex or irregular fault structures. Under such conditions, by incorporating structural priors and adopting a staged modeling strategy, the proposed method can effectively enhance the continuity and geological plausibility of the fault detection results, thus demonstrating superior performance in fault structure characterization and generalization stability, while showing promising potential for practical applications.

To further evaluate the sensitivity of the proposed method to prior information, two sets of experiments are conducted. First, the influence of the coherence prior on model performance is analyzed by varying the window size used in the computation of the coherence attribute. Specifically, window sizes of 3, 5, 7, 9, and 11 are considered, and the corresponding F1-score and IoU metrics are evaluated on the test dataset. The resulting trends are shown in Fig. 14(a). The results indicate that, as the window size increases, both metrics exhibit a gradual downward trend. This suggests that the coherence attribute computation parameters influence fault identification performance; however, the overall variation remains moderate. These observations demonstrate that the proposed method is robust to the choice of prior parameter settings and does not exhibit excessive sensitivity to a specific configuration, thereby confirming the stability of the two-stage framework when incorporating coherence-based priors.

Second, to analyze the sensitivity of the second stage to the quality of the first-stage output, different levels of random false-positive (FP) noise are injected into the fault probability volume produced by the first stage, and the perturbed results are used as inputs to the second stage. Specifically, FP injection ratios of 0%, 2%, 4%, 6%, 8%, and 10% are considered, and the corresponding F1-score and IoU metrics are evaluated on the test dataset. The resulting trends are illustrated in Fig. 14(b). The results show that both F1-score and IoU gradually decrease as the FP ratio increases; however, the overall performance degradation remains limited. This indicates that the second stage is able to re-model fault structures by jointly leveraging fault probability guidance and the original seismic data, exhibiting a certain degree of error correction capability and robustness, rather than simply amplifying errors propagated from the first stage. Considering both sensitivity analyses, the proposed method maintains stable fault identification performance under variations or inaccuracies in prior information, demonstrating its reliability and robustness in practical applications.

Although the proposed method demonstrates good stability and generalization performance on both synthetic and field seismic data, several limitations remain. First, the method relies on manually computed prior information, such as coherence attributes, whose effectiveness is to some extent influenced by parameter selection and data quality. Further investigation into adaptive or learning-based structural attributes is therefore warranted. Second, compared with single-stage approaches, the two-stage framework introduces additional computational overhead, which could be mitigated through parameter sharing or lightweight network design in future implementations. In addition, the current experimental validation is conducted on datasets of limited scale, and the applicability of the proposed method to larger-scale datasets and more complex geological settings requires further evaluation. Future work will focus on assessing the generalization capability of the method under complex structural scenarios (e.g., strike-slip faults and overthrust nappes) and large-scale datasets, as well as exploring the integration of fault strike and dip constraints and higher-level semantic information to further enhance the reliability of fault identification.

6. Conclusion

Motivated by the limited generalization capability and insufficient recognition stability of deep learning–based fault identification methods when applied to complex field seismic data, we propose a two-stage fault recognition framework guided by

coherence-based prior information. The proposed method is inspired by the rough-to-precise analysis strategy commonly adopted in manual fault interpretation, and employs two collaboratively operating prior-guided stages to achieve a preliminary characterization of the overall spatial distribution of faults, followed by fine modeling within the previously identified fault regions. Through this progressive process, the spatial continuity and structural consistency of fault features are gradually enhanced, thereby improving the stability and generalization performance of the model on field seismic data. Experimental results show that although some single-stage methods achieve higher quantitative metrics on synthetic data, their identification performance degrades when applied to field seismic data. In contrast, the proposed method demonstrates more stable and consistent performance under different geological conditions and is capable of delineating fault distributions with improved spatial continuity and more reasonable structures. Overall, the proposed two-stage fault recognition framework provides an effective approach for enhancing the applicability of deep learning–based methods to field seismic data and shows promising potential for practical applications.

CRediT authorship contribution statement

Jiang-Tao Ma: Writing – original draft, Validation, Methodology, Formal analysis. **Yang Liu:** Writing – review & editing, Supervision, Funding acquisition. **Suo-Liang Chang:** Writing – review & editing, Funding acquisition. **Nian-Xu Xi:** Investigation, Data curation. **Ding-Ding Deng:** Visualization, Data curation. **Xi Di:** Formal analysis, Data curation.

Declaration of competing interest

The authors declare that they have no known competing financial interests or personal relationships that could have appeared to influence the work reported in this paper.

Acknowledgments

This work was supported by the National Key Research and Development Program of China under Contract 2024YFC2909402.

References

Al-Dossary, S.A., Marfurt, K.J., 2003. Improved 3-D Seismic edge-detection Filter Applied to Vinton Dome Louisiana. SEG Technical Program Expanded Abstracts, pp. 2370–2372. https://doi.org/10.1190/1.1817846.

Bahorich, M., Farmer, S., 1995. 3-D seismic discontinuity for faults and stratigraphic features: the coherence cube. Lead. Edge 14 (10), 1053–1058. https://doi.org/10.1190/1.1437077.

Bangs, N.L., Mcintosh, K.D., Silver, E.A., et al., 2016. A recent phase of accretion along the southern Costa Rican subduction zone. Earth Planet Sci. Lett. 443, 204–215. https://doi.org/10.1016/j.epsl.2016.03.008.

Bashir, Y., Akdeniz, D.N., Balci, D., et al., 2025. 3D geo-seismic data enhancement leveraging geophysical attributes for hydrocarbon prospect and geological illumination. Phys. Chem. Earth, Parts A/B/C 138, 103854. https://doi.org/10.1016/j.pce.2025.103854.

Bashir, Y., Zahari, M.A.A.B., Karaman, A., et al., 2024. Artificial intelligence and 3D subsurface interpretation for bright spot and channel detections. AIMS Geosciences 10 (4), 662–683. https://doi.org/10.3934/geosci.2024034.

Chen, G., Liu, Y., 2021. Research progress of automatic fault recognition based on artificial intelligence. Prog. Geophys. 36 (1), 119–131. https://doi.org/10.6038/pg2021EE0252 (in Chinese).

Dosovitskiy, A., Beyer, L., Kolesnikov, A., et al., 2020. An Image Is Worth 16x16 Words: Transformers for Image Recognition at scale. arXiv preprint arXiv:2010.11929. https://doi.org/10.48550/arXiv.2010.11929.

Gao, K., 2024. Iterative multitask learning and inference from seismic images. Geophys. J. Int. 236 (1), 565–592. https://doi.org/10.1093/gji/ggad424.

Gao, K., Huang, L., Zheng, Y., 2022a. Fault detection on seismic structural images using a nested residual u-net. IEEE Trans. Geosci. Rem. Sens. 60, 1–15. https://doi.org/10.1109/TGRS.2021.3073840.

Gao, K., Huang, L., Zheng, Y., et al., 2022b. Automatic fault detection on seismic images using a multiscale attention convolutional neural network. Geophysics 87 (1), N13–N29. https://doi.org/10.1190/geo2020-0945.1.

Gersztenkorn, A., Marfurt, K.J., 1999. Eigenstructure-based coherence computations as an aid to 3-D structural and stratigraphic mapping. Geophysics 64 (5), 1468–1479. https://doi.org/10.1190/1.1444651.

Hatamizadeh, A., Yang, D., Roth, H.R., et al., 2021. UNETR: transformers for 3D medical image segmentation. arXiv preprint arXiv:2103.10504. https://doi.org/10.48550/arXiv.2103.10504.

Hu, L., Zheng, X., Duan, Y., et al., 2019. First-arrival picking with a U-Net convolutional network. Geophysics 84 (6), U45–U57. https://doi.org/10.1190/geo2018-0688.1.

Huang, L., Dong, X., Clee, E., 2017. A scalable deep learning platform for identifying geologic features from seismic attributes. Lead. Edge 36 (3), 249–256. https://doi.org/10.1190/tle36030249.1.

Jiang, F., Norlund, P., 2021. Assisted Fault Interpretation by multi-scale Dilated Convolutional Neural Network. European Association of Geoscientists & Engineers, pp. 1–5. https://doi.org/10.3997/2214-4609.202112679.

Kazmi, H.S., Ahmad, S., Shafiq, A., et al., 2012. Fault Characterization Using Volumetric Curvature from Continuous Phase Spectrum. SEG Technical Program Expanded Abstracts, pp. 1–5. https://doi.org/10.1190/segam2012-0445.1.

Li, N., Wang, L.Y., Huang, S.B., et al., 2019. 3D seismic fine structural interpretation in complex fault zones based on the high-definition ant-tracking attribute volume. Oil Geophys. Prospect. 54 (1), 182–190. https://doi.org/10.13810/j.cnki.issn.1000-7210.2019.01.021 (in Chinese).

Li, Z.W., Zhu, P.M., Zhang, H., et al., 2024. 3D fault identification based on MultiRes-Unet neural network. Geophys. Prospect. Pet. 63 (1), 91–103. https://doi.org/10.12431/issn.1000-1441.2024.63.01.008 (in Chinese).

Liu, Z., Lin, Y., Cao, Y., et al., 2021. Swin Transformer: Hierarchical Vision Transformer Using Shifted Windows. IEEE/CVF International Conference on Computer Vision, pp. 9992–10002. https://doi.org/10.1109/ICCV48922.2021.00986.

Marfurt, K.J., Kirlin, R.L., Farmer, S.L., et al., 1998. 3-D seismic attributes using a semblance-based coherency algorithm. Geophysics 63 (4), 1150–1165. https://doi.org/10.1190/1.1444415.

Mustafa, A., Rastegar, R., Brown, T., et al., 2024. Visual attention-guided learning with incomplete labels for seismic fault interpretation. IEEE Trans. Geosci. Rem. Sens. 62, 1–12. https://doi.org/10.1109/TGRS.2024.3370037.

Oktay, O., Schlemper, J., Folgoc, L.L., et al., 2018. Attention U-Net: learning where to look for the pancreas. arXiv preprint arXiv:1804.03999. https://doi.org/10.48550/arXiv.1804.03999.

Pan, S.J., Yang, Q., 2010. A survey on transfer learning. IEEE Trans. Knowl. Data Eng. 22 (10), 1345–1359. https://doi.org/10.1109/TKDE.2009.191.

Pramanik, P., Roy, A., Cuevas, E., et al., 2024. DAU-Net: dual attention-aided U-Net for segmenting tumor in breast ultrasound images. PLoS One 19 (5), e0303670. https://doi.org/10.1371/journal.pone.0303670.

Rich, C., 1997. Multitask learning. Mach. Learn. 28 (1), 41–75. https://doi.org/10.1023/A:1007379606734.

Ronneberger, O., Fischer, P., Brox, T., 2015. U-Net: convolutional networks for biomedical image segmentation. Medical Image Computing and Computer-Assisted Intervention 234–241. https://doi.org/10.1007/978-3-319-24574-4_28.

Sebastian, R., 2017. An overview of multi-task learning in deep neural networks. arXiv preprint arXiv:1706.05098. https://doi.org/10.48550/arXiv.1706.05098.

Tang, Z., Wu, B., Wu, W., et al., 2023. Fault detection via 2.5D transformer U-Net with seismic data pre-processing. Remote Sens. 15 (4), 1039. https://doi.org/10.3390/rs15041039.

Vaswani, A., Shazeer, N., Parmar, N., et al., 2017. Attention is all you need. arXiv preprint arXiv:1706.03762. https://doi.org/10.48550/arXiv.1706.03762.

Wu, W.H., Yang, Y., Wu, B.Y., et al., 2023. MTL-FaultNet: seismic data reconstruction assisted multitask deep learning 3-D fault interpretation. IEEE Trans. Geosci. Rem. Sens. 61, 1–15. https://doi.org/10.1109/TGRS.2023.3299378.

Wang, W., Chen, C., Ding, M., et al., 2021c. TransBTS: multimodal brain tumor segmentation using transformer. arXiv preprint arXiv:2103.04430. https://doi.org/10.48550/arXiv.2103.04430.

Wang, W., Mcmechan, G.A., Ma, J., et al., 2021b. Automatic velocity picking from semblances with a new deep-learning regression strategy: Comparison with a classification approach. Geophysics 86 (2), U1–U13. https://doi.org/10.1190/geo2020-0423.1.

Wang, J., Zhang, J.H., Zhang, J.L., et al., 2021a. Research on fault recognition method combining 3d res-unet and knowledge distillation. Appl. Geophys. 18 (2), 199–212. https://doi.org/10.1007/s11770-021-0894-2.

Wu, X., Geng, Z., Shi, Y., et al., 2020. Building realistic structure models to train convolutional neural networks for seismic structural interpretation. Geophysics 85 (4), WA27–WA39. https://doi.org/10.1190/geo2019-0375.1.

Wu, X., Liang, L., Shi, Y., et al., 2019a. FaultSeg3D: using synthetic data sets to train an end-to-end convolutional neural network for 3D seismic fault segmentation. Geophysics 84 (3), IM35–IM45. https://doi.org/10.1190/geo2018-0646.1.

Wu, X., Liang, L., Shi, Y., et al., 2019b. Multitask learning for local seismic image processing: fault detection, structure-oriented smoothing with edge-preserving, and seismic normal estimation by using a single convolutional neural network. Geophys. J. Int. 219 (3), 2097–2109. https://doi.org/10.1093/gji/ggz418.

Xiong, W., Ji, X., Ma, Y., et al., 2018. Seismic fault detection with convolutional neural network. Geophysics 83 (5), O97–O103. https://doi.org/10.1190/geo2017-0666.1.

Yan, Z., Gu, H., Cai, C., 2013. Automatic fault tracking based on ant colony algorithms. Comput. Geosci. 51, 269–281. https://doi.org/10.1016/j.cageo.2012.08.003.

Yang, W., He, Z.H., Chen, X.H., 2011. Application of three-dimensional volumetric curvature attributes to fault identification. Prog. Geophys. 26 (1), 110–115. https://doi.org/10.3969/j.issn.1004-2903.2011.01.011 (in Chinese).

Zhang, Q.H., Yang, L., 2015. Application of an improved ant colony in faults tracking. In: 2015 8th International Symposium on Computational Intelligence and Design, pp. 547–550. https://doi.org/10.1109/ISCID.2015.75.

Zhang, W., Wu, X., Wang, G., 2024. Enhancing deep learning for seismic interpretation with constraints from seismic attributes: a fault detection case study. IEEE Trans. Geosci. Rem. Sens. 62, 1–15. https://doi.org/10.1109/TGRS.2024.3471924.

Zhang, Z., Liu, Q., Wang, Y., 2018. Road extraction by deep residual U-Net. IEEE Geosci. Remote Sens. Lett. 15 (5), 749–753. https://doi.org/10.1109/LGRS.2018.2802944.

Zhou, T., Ma, Y., Sui, Y., et al., 2024. Fault transformer: an automatic fault detection algorithm on seismic images using a transformer enhanced neural network. Interpretation 12 (3), SE55–SE64. https://doi.org/10.1190/INT-2023-0120.1.